

Dielectrowetting actuation of droplet: Theory and experimental validation

Yayan Huang(黄亚俨), Rui Zhao(赵瑞), Zhongcheng Liang(梁忠诚), Yue Zhang(张月), Meimei Kong(孔梅梅), and Tao Chen(陈陶)

Citation: Chin. Phys. B, 2021, 30 (**10**): 106801. DOI: 10.1088/1674-1056/ac1926
Journal homepage: http://cpb.iphy.ac.cn; http://iopscience.iop.org/cpb

What follows is a list of articles you may be interested in

Molecular simulation study of the adhesion work for water droplets on water monolayer at room temperature

Mengyang Qu(屈孟杨), Bo Zhou(周波), and Chunlei Wang(王春雷)
Chin. Phys. B, 2021, 30 (**10**): 106804. DOI: 10.1088/1674-1056/ac192d

The drying of liquid droplets

Zechao Jiang(姜泽超), Xiuyuan Yang(杨修远), Mengmeng Wu(吴萌萌), Xingkun Man(满兴坤)
Chin. Phys. B, 2020, 29 (**9**): 096803. DOI: 10.1088/1674-1056/ab8ac7

Approximate expression of Young's equation and molecular dynamics simulation for its applicability

Shu-Wen Cui(崔树稳), Jiu-An Wei(魏久安), Wei-Wei Liu(刘伟伟), Ru-Zeng Zhu(朱如曾), Qian Ping(钱萍)
Chin. Phys. B, 2019, 28 (**1**): 016801. DOI: 10.1088/1674-1056/28/1/016801

The properties of surface nanobubbles formed on different substrates

Zheng-Lei Zou(邹正磊), Nan-Nan Quan(权楠楠), Xing-Ya Wang(王兴亚), Shuo Wang(王硕), Li-Min Zhou(周利民), Jun Hu(胡钧), Li-Juan Zhang(张立娟), Ya-Ming Dong(董亚明)
Chin. Phys. B, 2018, 27 (**8**): 086803. DOI: 10.1088/1674-1056/27/8/086803

Analysis of meniscus beneath metastable droplets and wetting transition on micro/nano textured surfaces

Yanjie Li(李艳杰), Xiangqin Li(李香琴), Tianqing Liu(刘天庆), Weiguo Song(宋伟国)
Chin. Phys. B, 2018, 27 (**8**): 086801. DOI: 10.1088/1674-1056/27/8/086801

Dielectrowetting actuation of droplet: Theory and experimental validation*

Yayan Huang(黄亚俨)[1], Rui Zhao(赵瑞)[1,†], Zhongcheng Liang(梁忠诚)[1,‡], Yue Zhang(张月)[2], Meimei Kong(孔梅梅)[1], and Tao Chen(陈陶)[1]

[1] *The Microfluidic Optical Technology Research Center, School of Electronic and Optical Engineering, Nanjing University of Posts and Telecommunications, Nanjing* 210023, *China*
[2] *Beijing Institute of Space Mechanics & Electricity, Beijing* 100094, *China*

(Received 21 April 2021; revised manuscript received 7 July 2021; accepted manuscript online 30 July 2021)

A theoretical model based on energy conversation is constructed to characterize the contracting behavior of the non-conductive droplet actuated by the dielectric effect in an immiscible dielectric liquid. To verify the theory, COMSOL is employed to simulate the evolution of the droplet based on dielectrowetting, and a measurement platform is established to monitor the change process of the droplet profile. The contact angle and the height of the droplet increase linearly up to 48° and 2.03 mm respectively when U ranges from 55 V to 160 V, while the droplet remained stationary when $U < 55$ V. The relative experimental results coincide with the prediction of theory and the simulation analysis.

Keywords: dielectrowetting, contact angle, height, COMSOL, droplet

PACS: 68.08.Bc, 68.03.Hj, 68.05.−n **DOI:** 10.1088/1674-1056/ac1926

1. Introduction

Microfluidic controlling technology plays a critical role in micro-total analysis systems or lab-on-a-chip systems.[1–3] The controllable adjustment of the microfluidic can be realized by various methods, including thermal,[4] mechanical force,[5] dielectrowetting,[6–8] electrowetting,[9–19] and so on. Electrowetting technology has been found numerous potential applications in prism,[11,12] liquid lens,[13] displays,[14] lab-on-a-chip,[15] and light valve.[16] However, it still has some limitations, such as demand of conducting fluid, contact angle saturation and electrolysis, which affects its application and development.[20,21]

Unlike electrowetting, dielectrowetting is a technology that applies a non-uniform electric field to control the wettability of a non-conductive liquid, which avoids electrolysis, joule heating, microbubbles, *etc.*[22] Benefiting from the above advantages, dielectrowetting technology receives extensive attention and research in recent years. In 2006, Cheng *et al.* demonstrated a miniature droplet lens depending on dielectrowetting effects, whose focal length ranged from 1.6 mm to 2.6 mm in 220 ms.[23] In 2010, Tsai and Yeh proposed a liquid iris diaphragm by using dielectric force, whose aperture could vary from 4 mm to 1.5 mm at 160 V·rms.[24] In 2011, McHale *et al.* put forward how dielectrowetting reduce the contact angle of a droplet by interdigital electrode.[25] In 2017, Geng *et al.* reported four droplet operations (creating, transporting, splitting, and merging of droplets) by aid of dielectrowetting technology.[6] In 2018, Kim *et al.* presented a novel light steering device operated by dielectrowetting actuation for diverse optical applications.[26] In 2021, Liang *et al.* developed a dielectrowetting-based optofluidic phase modulator by wheel spoke coplanar-electrode, its optical phase modulation can reach 9.366π when the voltage reached 150 V.[27] These works provided references and guides for dielectrowetting-based devices design, however, the contracting feature of the droplets actuated by dielectrowetting and the mechanisms involved remain obscure.

In this paper, we analyze the wettability property of an insulating droplet under the action of dielectric effect generated by the wheel spoke coplanar-electrode. Based on energy conversation, a theoretical model is constructed to predict the transient contact angle and the height of the droplet at different voltages. In the meantime, the evolution of the droplet contracting is simulated by COMSOL, and a measurement platform is established to monitor the change process of the droplet profile. Series of experiments are carried out to verify the prediction of theory and the simulation of COMSOL.

2. Theoretical analysis

Figure 1 describes the force balance of silicone oil droplet surrounded by glycol near three-phase contact line during dielectrowetting evolution, where γ_{LF}, γ_{SF}, and γ_{SF} are the

*Project supported by the National Natural Science Foundation of China (Grant No. 61775102) and the Youth Program of the National Natural Science Foundation of China (Grant No. 61905117).

†Corresponding author. E-mail: zhaor@njupt.edu.cn
‡Corresponding author. E-mail: zcliang@njupt.edu.cn

© 2021 Chinese Physical Society and IOP Publishing Ltd

surface tensions at the silicone oil/glycol interface, silicone oil/substrate interface, and glycol/substrate interface respectively; θ is the equilibrium contact angle, f_s is the pinning force, F_e is the dielectric field force of an electrically neutral object in an uneven electric field,[25] f_v is the viscous friction force, f_{dyn} is the dynamic friction force. When the dielectric field force F_e is not stronger enough to against the pinning force,[28,29] the droplet remains stationary, *i.e.*, it is in static state. Hence the apparent contact angle remains unchanged as shown in Fig. 1(a). Once the electric field force F_e exceeds the maximum pinning friction f_s, the droplet begins to move, and the apparent contact angle begins to increase and eventually evolves into the moving state as shown in Fig. 1(b). Here the transition from the static state to the moving state depends on the dielectric field force F_e, *i.e.*, the threshold voltage U_{th}.

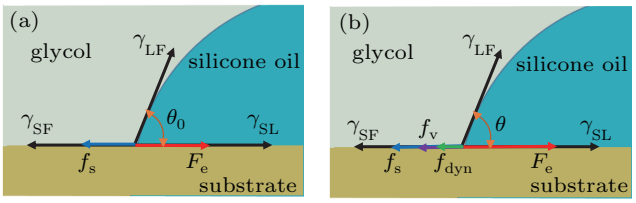


Fig. 1. Sketch of force balance at three-phase line in dielectrowetting evolution: (a) in static state and (b) in moving state.

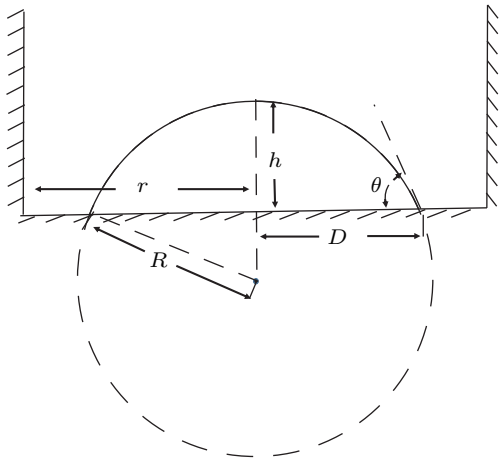


Fig. 2. Diagram of silicone oil droplet with radius R and contact angle θ.

The droplet illustrated in Fig. 2 is assumed to remain spherical during the dielectrowetting evolution. According to the calculation formulas of the volume and area for the spherical cap, the following relationships can be achieved:

$$V_0 = \pi h^2\left(R-\frac{h}{3}\right) = \frac{\pi h(3D^2+h^2)}{6}, \tag{1}$$

$$h = R(1-\cos\theta), \tag{2}$$

$$A_s = 2\pi Rh, \tag{3}$$

$$A_b = D^2\pi, \tag{4}$$

$$A_g = \left(r^2-D^2\right)\pi, \tag{5}$$

where V_0 is the volume of silicone oil droplet, θ is the contact angle, h is the height of the droplet, R is the spherical radius of the droplet, D is the contact radius among substrate and droplet, r is the radius of the cavity, A_s is the interface area of the silicone oil/glycol, A_b is the interface area of the substrate/silicone oil, and A_g is the interface area of the substrate/glycol.

In the static state, the silicone oil/glycol surface tension energy (W_s), silicone oil/substrate surface tension energy (W_b), and glycol/substrate surface tension energy (W_g) can be respectively given as follows:

$$W_s = A_s \times \gamma_{LF} = 2\pi Rh\gamma_{LF}, \tag{6}$$

$$W_b = A_b \times (\gamma_{SF}-f_s) = D^2\pi(\gamma_{SF}-f_s), \tag{7}$$

$$W_g = A_g \times \gamma_{SF} = \left(r^2-D^2\right)\pi\gamma_{SF}. \tag{8}$$

Since the distribution of the dielectric field force depends on electrode structure, electrode polarity, and the interface area between electrode and droplet, the dielectric energy W_E generated by electric field can be represented as[30,31]

$$W_E = -\left(\frac{A_rA_a}{(A_r+A_a)A_t}\right)\frac{\varepsilon_0(\varepsilon_L-\varepsilon_F)D^2\pi U^2}{2\delta}, \tag{9}$$

where δ is penetration depth of electric field, ε_L, ε_F, and ε_0 are the relative permittivities of the silicone oil, glycol, and the dielectric constant in a vacuum respectively; A_a, A_r, and A_t denote cover area of the droplet above the driving electrode, the reference electrode, and the entire electrode respectively. The electrode structure designed in this work is the wheel spoke coplanar–electrode structure as shown in Fig. 3(b).

The total interfacial potential energy W_T can be written as the sum of W_s, W_b, W_g, and W_E,

$$\begin{aligned} W_T &= 2\pi Rh\gamma_{LF}+D^2\pi(\gamma_{SF}-f_s)+(r^2-D^2)\pi\gamma_{SF} \\ &\quad +A\frac{\varepsilon_0\Delta\varepsilon D^2\pi U^2}{2\delta}, \end{aligned} \tag{10}$$

where $\Delta\varepsilon = (\varepsilon_F-\varepsilon_L)$, $A = A_rA_a/(A_r+A_a)A_t$.

Rearranging the Young's equation[32] leads to

$$\gamma_{SF} = \gamma_{SF}+\gamma_{LF}\cos\theta_0, \tag{11}$$

here θ_0 is the initial contact angle of the droplet.

Substituting Eq. (11) into Eq. (10) yields

$$\begin{aligned} W_T &= (2\pi Rh-D^2\pi\cos\theta_0)\gamma_{LF}+r^2\pi\gamma_{SF}-D^2\pi f_s \\ &\quad +A\frac{\varepsilon_0\Delta\varepsilon D^2\pi U^2}{2\delta}. \end{aligned} \tag{12}$$

With the help of Eq. (1), equation (12) can be derived as

$$\begin{aligned} W_T &= \left[\frac{2\pi h^3+6V_0}{3h}-\frac{(6V_0-\pi h^3)\cos\theta_0}{3h}\right]\gamma_{LF} \\ &\quad +r^2\pi\gamma_{SF}\left(A\frac{\varepsilon_0\Delta\varepsilon U^2}{2\delta}-f_s\right)\left(\frac{6V_0-\pi h^3}{3h}\right). \end{aligned} \tag{13}$$

The dielectrowetting system satisfies the law of energy conservation once the droplet reaches equilibrium, hence one can have $\mathrm{d}W_\mathrm{T}/\mathrm{d}h = 0$, and

$$\left[\frac{12\pi h^3 - 18V_0}{9h^2} + \frac{(18V_0 + 6\pi h^3)\cos\theta_0}{9h^2}\right]\gamma_{\mathrm{LF}} - \left(A\frac{\varepsilon_0\Delta\varepsilon U^2}{2\delta} - f_\mathrm{s}\right)\left(\frac{18V_0 + 6\pi h^3}{9h^2}\right) = 0. \tag{14}$$

Substituting Eq. (1) into Eq. (14), equation (14) can be written as

$$\cos\theta = \cos\theta_0 - A\frac{\varepsilon_0\Delta\varepsilon U^2}{2\delta\gamma_{\mathrm{LF}}} + \frac{f_\mathrm{s}}{\gamma_{\mathrm{LF}}}. \tag{15}$$

As mentioned above, when voltage ranges from 0 V to U_th, the contact line does not move and the contact angle remains unchanged, the pinning force f_s in Eq. (15) can be represented by

$$f_\mathrm{s} = A\frac{\varepsilon_0\Delta\varepsilon U^2}{2\delta}. \tag{16}$$

Combined with Eq. (16), equation (15) is simplified as

$$\cos\theta = \cos\theta_0. \tag{17}$$

Equation (17) succeeds to describe the dielectrowetting evolution of the droplet in static state.

Once the voltage increases and exceeds the threshold U_th, the dielectrowetting process evolves into the moving state. At this stage, the three-phase contact line begins to move and then the droplets began to contract inward. The dynamic contact line friction force f_dyn is[33]

$$f_\mathrm{dyn} = \zeta X, \tag{18}$$

where ζ is the coefficient of contact line friction, and X is the moving velocity of contact line.

The viscous friction force f_v is linear with the velocity of droplet[34,35]

$$f_\mathrm{v} = 6\mu X, \tag{19}$$

here μ is the viscosity of silicone oil droplet.

The relationship between moving velocity of the contact line X in Eq. (18) and voltage U is given as follows:[36,37]

$$X = k_1\frac{\gamma_{\mathrm{LF}}}{\mu}\left(\cos\theta_0 - \frac{CU^2}{2\gamma_{\mathrm{LF}}} - \cos\theta\right), \tag{20}$$

where k_1 is a constant, $C = A(\varepsilon_0\Delta\varepsilon/2\delta)$ is the effective capacitance per unit.

The base tension energy W_b is expressed as

$$W_\mathrm{b} = D^2\pi(\gamma_{\mathrm{SF}} - f_\mathrm{dyn} - f_\mathrm{v} - c_\mathrm{pin}), \tag{21}$$

where c_pin is the maximum pinning force per unit area.

Accordingly, the interfacial potential energy can be represented as

$$W_\mathrm{T} = 2\pi Rh\gamma_{\mathrm{LF}} + D^2\pi(\gamma_{\mathrm{SF}} - f_\mathrm{s}) + (r^2 - D^2)\pi\gamma_{\mathrm{SF}} + A\frac{\varepsilon_0\Delta\varepsilon D^2\pi U^2}{2\delta}. \tag{22}$$

Set $\mathrm{d}W_\mathrm{T}/\mathrm{d}h = 0$, the following equation can be obtained:

$$\left[\frac{12\pi h^3 - 18V_0}{9h^2} + \frac{(18V_0 + 6\pi h^3)\cos\theta_0}{9h^2}\right]\gamma_{\mathrm{LF}} - \left(A\frac{\varepsilon_0\Delta\varepsilon U^2}{2\delta} - X(6\mu + \zeta) - c_\mathrm{pin}\right)\frac{18V_0 + 6\pi h^3}{9h^2} = 0. \tag{23}$$

Substituting Eqs. (1), (2), (18), (19), and (20) into Eq. (23) yields

$$\cos\theta = \cos\theta_0 - A\frac{\varepsilon_0\Delta\varepsilon U^2}{2\delta\gamma_{\mathrm{LF}}} + \frac{c_\mathrm{pin}}{\gamma_{\mathrm{LF}}} + \frac{k_1A(6\mu + \zeta)\varepsilon_0\Delta\varepsilon U^2}{2\mu\gamma_{\mathrm{LF}}\delta}. \tag{24}$$

The relationship between contact angle and voltage for the whole dielectrowetting process is given below:

$$\cos\theta = \begin{cases} \cos\theta_0, \\ \cos\theta_0 - A\dfrac{\varepsilon_0\Delta\varepsilon U^2}{2\delta\gamma_{\mathrm{LF}}} + \dfrac{c_\mathrm{pin}}{\gamma_{\mathrm{LF}}} + \dfrac{k_1A(6\mu+\zeta)\varepsilon_0\Delta\varepsilon U^2}{2\mu\gamma_{\mathrm{LF}}\delta}, \end{cases} \tag{25}$$

where $K = k_1(6\mu + \zeta)$ is determined by fitting the equation to the experimental data at the point of threshold potential.

Substituting Eq. (25) into Eq. (2), the height of droplet is achieved as follows:

$$h = \begin{cases} h_0, \\ \sqrt[3]{\dfrac{3V_0 - 3V_0\left(\cos\theta_0 - A\frac{\varepsilon_0\Delta\varepsilon\pi U^2}{2\delta\gamma_{\mathrm{LF}}} + \frac{c_\mathrm{pin}}{\gamma_{\mathrm{LF}}} + \frac{k_1A(6\mu+\zeta)\varepsilon_0\Delta\varepsilon U^2}{2\mu\gamma_{\mathrm{LF}}\delta}\right)}{\left(2 + \left(\cos\theta_0 - A\frac{\varepsilon_0\Delta\varepsilon\pi U^2}{2\delta\gamma_{\mathrm{LF}}} + \frac{c_\mathrm{pin}}{\gamma_{\mathrm{LF}}} + \frac{k_1A(6\mu+\zeta)\varepsilon_0\Delta\varepsilon U^2}{2\mu\gamma_{\mathrm{LF}}\delta}\right)\right)\pi}}. \end{cases} \tag{26}$$

The threshold voltages U_th in Eqs. (25) and (26) can be calculated theoretically with the aid of Eqs. (27) and (28) listed below.

When $U = U_\mathrm{th}$, the dielectrowetting force F_e is greater than the maximum pinning force c_pin,[38] which triggers the droplet to contract inward. Consequently

$$c_\mathrm{pin} = \gamma_{\mathrm{LF}}[\cos\theta_0 - \cos(\theta_0 + \alpha)] = \frac{CU_\mathrm{th}^2}{2}, \tag{27}$$

where α is the difference between advancing angle and receding angle. Rearranging Eq. (27), the threshold potential U_th is

written as

$$U_{\rm th} = \sqrt{\frac{2\gamma_{\rm LF}[\cos\theta_0 - \cos(\theta_0+\alpha)]}{C}}. \tag{28}$$

3. Experimental procedure

In Fig. 3, a 70-μL silicone oil droplet (Dow Corning 200 series) is deposited in the center of the substrate by a syringe pipette, which is placed in a clear acrylic cavity and immersed in an immiscible glycol liquid. The coplanar-electrode is designed as shown in Fig. 3(b), the corresponding radius of the two concentric circles is 5 mm and 15 mm respectively. The planar ITO electrode is coated with about 5-μm SU8 as a dielectric layer, and then about 400-nm hydrophobic layer. To keep the silicone oil droplet fixed in the center of the substrate, the fluoropel is only coated on the central area (∼ 20 mm in diameter). The relative parameters of liquids are listed in Table 1 (room temperature 20 °C).[39]

Table 1. Parameters of liquid medium.

	Dimethyl silicone oil	Ethylene glycol
Density (g/cm^3)	∼ 0.96	∼ 1.1155
Dielectric constant	∼ 2.17	∼ 44.1
Surface tension (mN/m)	∼ 15.9	∼ 46.49
Viscosity (mPa·s)	∼ 96	∼ 25.66

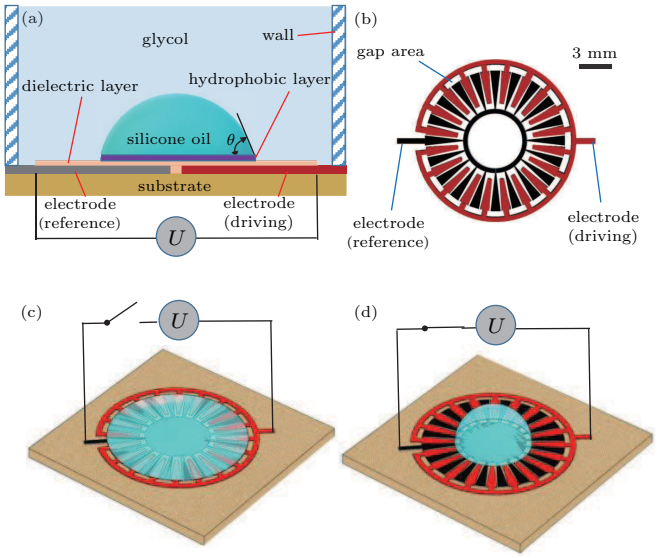


Fig. 3. Diagram and principle of dielectrowetting: (a) cross-section view; (b) wheel spoke coplanar–electrode structure (top view); (c) initial state; (d) contracting state.

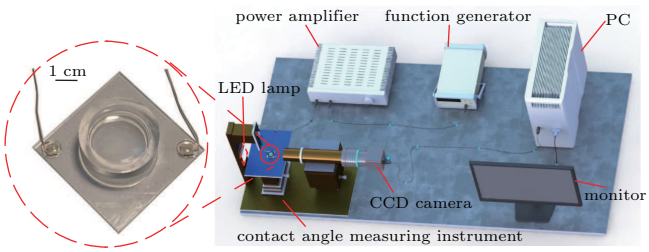


Fig. 4. Schematic diagram of measurement system.

Since the density of the two liquids is similar, the interface of the two liquids is assumed to be spherical. Here the working voltage is a sinusoidal AC signal with a frequency of 500 Hz. When the working voltage is bigger enough, the contact angle of the droplet increases and the shape of the droplet changes, which is corresponding to the contracting process from Fig. 3(c) to Fig. 3(d). The change of contact angle and the height of the droplet is monitored and measured with drop shape analysis systems (SCI3000F, shown in Fig. 4), which are repeated 3 times at fresh sample locations.

4. Results and discussion

Figures 5(e1)–5(e5) provides the changing profile of silicone oil droplet captured at 0 V, 40 V, 80 V, 120 V, 160 V respectively. When the voltage is in the range of 0 V–55 V, no obvious change in droplet profile. This stage is called the static state, and 55 V is defined as the voltage threshold. When the voltage increases up to 55 V, the droplet starts to contract inward and then evolves into the in moving state. Continuing increasing of voltage, visible change of contact angle and height of the silicone oil droplet can be seen in Figs. 5(e3)–5(e5) corresponding to U = 80 V, 120 V, 160 V respectively. When the voltage is 160 V, the contact angle of silicone oil droplet is 48° and the relevant stable height is 2.03 mm.

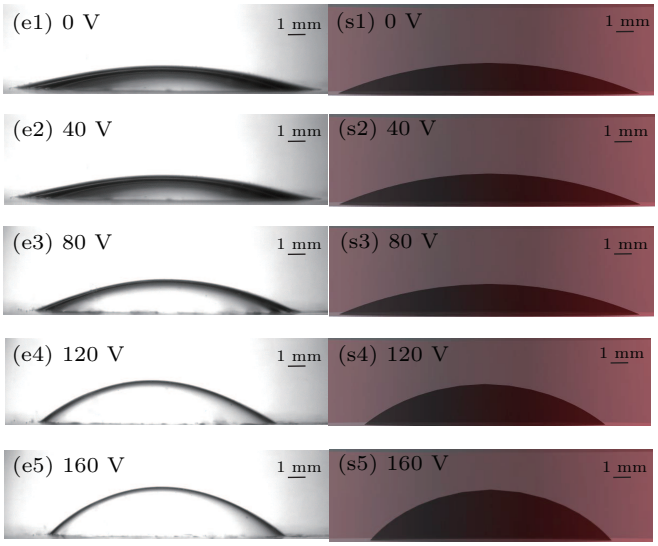


Fig. 5. The droplet profile changing during driven procedure: (e1)–(e5) captured by CCD camera, (s1)–(s5) simulated by COMSOL.

The contracting model based on Eq. (25) is constructed in COMSOL Multiphysics 5.4(a), and the relative parameters are provided in Table 2. The simulated profiles of droplet at different voltages are shown in Fig. 5(s1)–5(s5). Comparing the simulations with experiments, finally we get the simulation results that coincide with the experimental results.

The contact angle is plotted as line with hollow circle (◯) in Fig. 6. The line with hollow square (□) in Fig. 6 is the theoretical values predicted by Eq. (25), which shows good

consistence with our experimental results. When the voltage is smaller than 55 V, the droplet remains stationary and consequently the contact angle is constant. When the voltage reaches 55 V, the droplet begins to contract inward. When the voltage ranges from 55 V to 160 V, the corresponding transient contact angle increase linearly from 23° to 48°.

Substituting $\gamma_{LF} = 16.5$ mN/m, $\delta = 66$ μ m, $\varepsilon_0 = 8.85 \times 10^{-12}$, $\Delta\varepsilon = 42$, $\theta_0 = 23°$, $\alpha = 28°$ into Eq. (28), the theoretical threshold potential $U_{th} = 57$ V is achieved, which is almost close to the experimental threshold value 55 V.

Table 2. Parameters of simulation model parameters.

Parameter	Value	Instruction
D (mm)	10	cavity bottom radius
H (mm)	5	cavity height
R (mm)	19	radius of curvature of droplet
L (mm)	3	height of droplet Center
θ_0 (°)	20	zero voltage contact angle
Gamma (N/m)	0.0165	surface tension
Epsr	42	dielectric constant difference

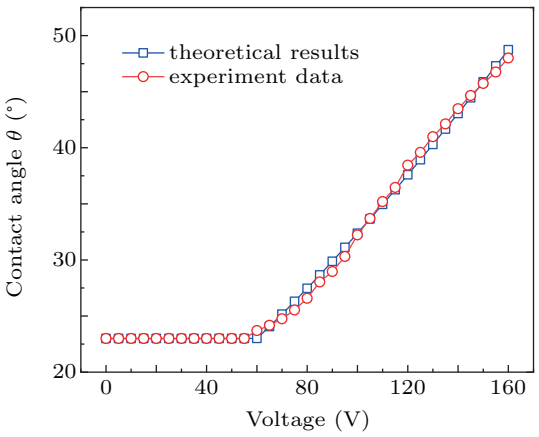


Fig. 6. Comparison of contact angle *versus* voltage among experimental data and theoretical results.

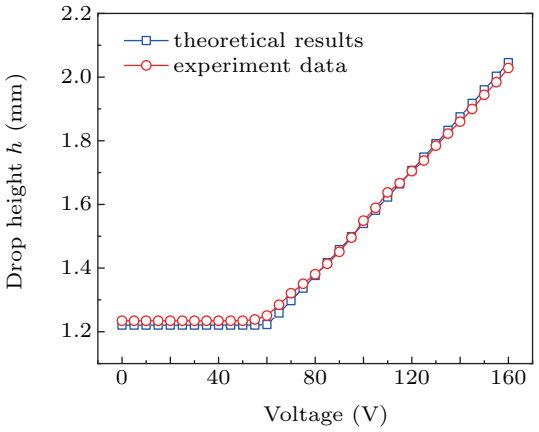


Fig. 7. The height of the droplet *versus* voltage.

Figure 7 illustrates the variation of stable height of the droplet at different voltage. The line with hollow circle (◯) represents the experimental data while the line with hollow square (□) denotes the theoretical values predicted by Eq. (26). There is no obvious change in height when voltage is smaller than 55 V. When the voltage increases from 55 V to 160 V, the height of the droplet increases from 1.23 mm to 2.03 mm, and the maximum height variation approaches to 0.8 mm. Our theoretical curve succeeds to predict the change of the height, which shows good agreement with the related experimental results.

5. Conclusion

The focus of this work is to study the dielectrowetting property of silicone oil droplet under the action of dielectric effect. A theoretical model based on energy conversation is established to predict the transient contact angle and the height of the droplet at different voltages. In the meantime, the dielectrowetting evolution of the droplet profile is simulated by COMSOL. Series of experiments are carried out to verify the prediction of theory and the simulation of COMSOL. As for the dielectrowetting process, it experiences two states, *i.e.*, the static state and the moving state. When the voltage is smaller than 55 V, the droplet remains stationary, *i.e.*, it is in the static state; when the voltage increases above 55 V, the droplet begins to contract, *i.e.*, it is in the moving state. The contact angle of the droplet increases linearly from 23° to 48° , and the relative height of the droplet changes from 1.23 mm and 2.03 mm when voltage U ranges from 55 V to 160 V.

References

[1] Murphy T W, Zhang Q, Naler L B, Ma S and Lu C 2018 *Analyst* **143** 60
[2] Li J 2020 *Lab on a Chip* **20** 1705
[3] Cui P and Wang S 2019 *Journal of Pharmaceutical Analysis* **9** 238
[4] Grigoriev R O 2005 *Phys. Fluids* **17** 033601
[5] Hongbin Y, Guangya Z, Siong C F and Feiwen L 2008 *Journal of Micromechanics and Microengineering* **18** 115016
[6] Geng H, Feng J, Stabryla L M and Cho S K 2017 *Lab on a Chip* **17** 1060
[7] Edwards A M J, Brown C V, Newton M I and McHale G 2018 *Current Opinion in Colloid & Interface Science* **36** 28
[8] Zhao R, Cumby B, Russell A and Heikenfeld J 2013 *Appl. Phys. Lett.* **104** 019901
[9] Ashtiani A O and Jiang H 2017 *Journal of Microelectromechanical Systems* **26** 305
[10] Kedzierski J, Berry S and Abedian B 2009 *Journal of Microelectromechanical Systems* **18** 845
[11] Chen T and Liang Z 2010 *Optoelectronic Devices and Integration III. International Society for Optics and Photonics* **7847** 78472
[12] Takei A, Iwase E, Hoshino K, Matsumoto K and Shimoyama I 2007 *Journal of Microelectromechanical Systems* **16** 1537
[13] Park I S, Park Y, Oh S H, Yang W J and Chung S K 2018 *Sensors and Actuators A: Physical* **273** 317
[14] You H and Steckl A J 2010 *Appl. Phys. Lett.* **97** 023514
[15] Chung S K, Zhao Y and Cho S K 2008 *Journal of Micromechanics and Microengineering* **18** 095009
[16] Yuan R Y, Luo L, Wang J H, Li L and Wang H 2018 *IEEE Photon. Technol. Lett.* **30** 1629
[17] Zhao R and Liang Z C 2016 *Chin. Phys. B* **25** 066801

[18] Zeng X F, Yue R F, Wu J G, Dong L and Liu L T 2006 *Chin. Phys. Lett.* **21** 1851
[19] Yue R F, Wu J G, Zeng X F, Kang M and Liu L T 2006 *Chin. Phys. Lett.* **23** 2303
[20] Quinn A, Sedev R and Ralston J 2005 *J. Phys. Chem. B* **109** 6268
[21] Nelson W C, Sen P and Kim C J 2011 *Langmuir* **27** 10319
[22] Vallet M, Berge B and Vovelle L 1996 *Polymer.* **37** 2465
[23] Cheng C C, Chang C A and Yeh J A 2006 *Opt. Express* **14** 4101
[24] Tsai C G and Yeh J A 2010 *Opt. Lett.* **35** 2484
[25] McHale G, Brown C V, Newton M I, Wells G G and Sampara N 2011 *Phys. Rev. Lett.* **107** 186101
[26] Kim D, Park Y, Lee D Y and Chung S K 2018 *IEEE Micro-Electro Mechanical Systems (MEMS)* pp. 585–587
[27] Liang Z C, Ding W X, Zhao R, Huang Y Y, Kong M M and Chen T 2021 *Langmuir* **37** 769
[28] Bizonne C C, Barrat J L, Bocquet L and Charlaix E 2003 *Nat. Materi.* **2** 237
[29] Cox R G 2006 *J. Fluid Mech.* **168** 169
[30] Burkhart C T, Maki K L and Schertzer M J 2020 *Langmuir* **36** 8129
[31] Yi U C and Kim C J 2006 *Journal of Micromechanics and Microengineering* **16** 2053
[32] Young T 1805 *Phil. Trans. Roy. Soc. London* **95** 65
[33] Ren H, Fair R B, Pollack M G and Shaughnessy E J 2002 *Sensors and Actuators B: Chemical* **87** 201
[34] Lin J L, Lee G B, Chang Y H and Lien K Y 2006 *Langmuir* **22** 484
[35] Cottin-Bizonne C, Barrat J L, Bocquet L and Charlaix E 2003 *Nat Mater* **2** 237
[36] McHale G, Brown C V and Sampara N 2013 *Nat. Commun.* **4** 1605
[37] Zhao Y P and Yuan Q 2015 *Nanoscale.* **7** 2561
[38] Chang J H and Park J J 2012 *J. Adhesion Sci. Technol.* **26** 2105
[39] Yang C Y, Ho F H, Wang P J and Yeh J A 2010 *Langmuir* **26** 6314